Annals of Warsaw University of Life Sciences – SGGW
Forestry and Wood Technology No. 111, 2020: 94-105
(Ann. WULS-SGGW, For. and Wood Technol. 111, 2020)

Modelling of nitrogen multi-energy ion implantation into WC-Co indexable knives for wood-based materials machining

MAREK BARLAK[1], JACEK WILKOWSKI[2], ZBIGNIEW WERNER[1]
[1] Plasma/Ion Beam Technology Division (FM2), National Centre for Nuclear Research Świerk – NCBJ
[2] Warsaw University of Life Sciences – SGGW, Institute of Wood Sciences and Furniture, Department of Mechanical Processing of Wood

Abstract: *Modelling of nitrogen multi-energy ion implantation into WC-Co indexable knives for wood-based materials machining.* The paper presents the results of the modelling of multi-energy ion implantation processes of nitrogen to WC-Co indexable knives for wood-based materials machining. The modelling was performed for implantation of N^{+}+N_2^{+} ions, for implanters without and with mass separation. Additionally, modelling for average charge state and for the extended implantation case was executed. The best results, i.e. flat and long plateau region and the most favourable plateau/multi ratio were obtained for N^{+} ions.

Keywords: WC-Co tools, multi-energy ion implantation, modelling, wood-based materials

INTRODUCTION

The cemented tungsten carbides – a combination of hard and brittle carbides and a relatively soft and ductile metallic binder, provides an exceptional combination of attractive material properties such as strength, hardness, fracture toughness, refractoriness, stiffness, resistance to compressive deformation and wear resistance at room temperature as well as at higher temperatures up to 400°C (Milman et al. 1997, Sheikh-Ahmad and Bailey 1999, Pirso et al. 2004, Bonny et al. 2004, Choi et al. 2010, Olovsjö et al. 2013). Unfortunately, the durability of tools made of this material is still insufficient. There are several methods to improve this property. The ion implantation is a relatively simple, cheap and fast way of improving tribological properties of machine parts or cutting tools (Barlak et al. 2016, Barlak et al. 2017). Implantation modifies the near-surface area. The modified region is not a layer; therefore problems with adhesion and dimensional change are missing. Therefore, ion implantation can be applied also for the modification of the tools ready to use (Straede 1996; Mikkelsen et al. 2002; Rodríguez et al. 2002). Unfortunately, the width of the modified region is small. For example, the values of the ion range and the range strangling are about 60 nm in the case of N^{+} ions implantation with the energy of 70 keV (author's own result). There are several ways to increase the range of the implanted ions, for example by the implantation of the elements with smaller atomic mass and/or by the introduction of the additional energy to the system e.g. by the heating of the implanted material (diffusion) (Fayeulle et al. 1986).

The multi-implantation, also referred to as multi-energy ion implantation, multiple energy ion implantation, multiple implantation or multi-step implantation are known for several decades and used mainly for the shaping electronic or optical structures, like "low-high-low structure", "box" profile or "horse head" type profile or for the creation of the plateau in the depth profile of the implanted elements and extension of their range (Dening and Weiyuan 1987, Magruder et al. 2001, Magruder et al. 2002, Naumova et al. 2003, Phelps G.J. 2004, Magruder et al. 2004,

Posselt et al. 2005, Fu et al. 2007, Tsuji et al. 2007, Piekoszewski et al. 2009, Wang et al. 2009, Werner et al. 2009, Zhao et al. 2010, Magruder et al. 2011, Zhang et al. 2013, Lazar et al. 2015, Becerra et al. 2017, Liu et al. 2018, Teranishi et al. 2018, Chen and Lin 2019, Wang et al. 2019, Zhao et al. 2019).

The multi-implantation is a sum of several typical ion implantation processes with the energy value decreasing in consecutive stage (David et al. 2002, Lazar et al. 2015). The decreasing energy value is very important from the point of view of the microstructure damage and the chemical changes of the implanted regions. The natural multi-implantation is the implantation of the ions with multiple charges, using non-mass separated implanter, but in this case, the user can't affect the energy or/and fluence of individual ions.

Dening and Weiyuan (Dening and Weiyuan 1987) proposed the "equivalent area" method, based on the integral calculus, for the determination of the multi-energy effect. The empirical way is a different approach to solve this problem. This paper presents our proposition of an approach to the modelling/determining a plateau in the depth profiles of nitrogen implanted to W-C-Co material, using two main types of ion implanters, i.e. the implanters without mass separation (with direct ion beam) and with mass separation (without direct ion beam) in which a homogenous ion beam in terms of constant e/m ratio is formed (Barlak et al. 2019). The theoretical solution of this issue will help in preparation of the actual adjusting a multi-process of e.g. WC-Co tools indexable knives, used to wood-based material machining.

MATERIAL AND METHODS

The modelling of multi-implantation included two stages. In the first stage, the classical depth profiles of nitrogen in W-C-Co substrate were modelled for the accelerating voltage from 10 to 70 kV (typical values for classical ion implanters) with a step of 5 kV. In the second stage, the modelled profiles were exported to Microsoft Excel 2010 spreadsheet and collated for the selection, the addition and the determination of the fluences of the individual ion implantation processes.

The Stopping and Range of Ions in Matter (SRIM-2013.00), freeware type code was used for modelling of the depth profiles of nitrogen implanted to W-C-Co material (SRIM 2019, Zhang et al. 1998, Barlak et al. 2019a, Barlak et al. 2019b, Barlak et al. 2019c, Barlak et al. 2019d). The modelling was performed for 100 000 implanted ions of nitrogen. The angle of the ion incidence was defined as 0° (perpendicular to the implanted target). The simulations were performed for room temperature implantation. The modelling did not account for the phenomenon of substrate sputtering by the implanted ions, substrate damages and the chemical reactions between the implanted nitrogen and the substrate components.

W-C-Co of a composition: 90.86% of tungsten, 5.94% of carbon and 3.2% of cobalt in weight percentages i.e. 47.4% of tungsten, 47.4% of carbon and 5.2% of cobalt in atomic percentages was defined as a target. Its density, adopted for the simulation was 15.2 g/cm^3. This value was declared by the knives supplier (KCR08 type knives, by Ceratizit, Austria).

Four kinds of processes were considered, i.e.: N^++N_2^+ ion beam and the corresponding to him, the average charge state (ACS) case - for the ion implanters without mass separation and N^+ and N_2^+ ion beams - both for the implanters with mass separation. Nitrogen ion beam generated by an ion implanter with direct beam contains two kinds of ions, i.e. N^+ and N_2^+, in the ratio ~1:1, so there are two elementary charges per three atoms. Likewise, the average charge state is at the level of 0.67 (Barlak et al. 2019).

Table 1 presents the ion energy values corresponding to the values of acceleration voltage for all considered cases of nitrogen beam. These values were used for modelling of the classical depth profiles.

The values of the peak volume dopant concentrations N_{max} for the implanted fluence of 1e17 cm^{-2}, the projected range R_p, the range straggling ΔR_p, the kurtosis and the skewness were determined for all nitrogen profiles, i.e. N^++N_2^+, ACS, N^+ and N_2^+. In the next step, the modelled profiles were collated in the spreadsheet and the example multi-implantation profiles were empirically determined for the total implanted fluence of 1e17 cm^{-2}.

Table 1. The ion energy values corresponding to the values of acceleration voltage for all considered cases of nitrogen beam

Acceleration voltage (kV)	Kind of implanted ions			
	Implanter without mass separation		Implanter with mass separation	
	N^++N_2^+ (50%+50%)	ACS (100%)	N^+ (100%)	N_2^+ (100%)
	Energy (keV)			
10	10+5	6.7	10	5
15	15+7.5	10.05	15	7.5
20	20+10	13.4	20	10
25	25+12.5	16.75	25	12.5
30	30+15	20.1	30	15
35	35+17.5	23.45	35	17.5
40	40+20	26.8	40	20
45	45+22.5	30.15	45	22.5
50	50+25	33.5	50	25
55	55+27.5	36.85	55	27.5
60	60+30	40.2	60	30
65	65+32.5	43.55	65	32.5
70	70+35	46.9	70	35

Next, the plateau was determined for all multi-profiles. The minimum value for "flat" part of the profiles determined the boundaries of plateau (thickness of plateau). The average value of plateau, standard deviation and standard error for this average value were calculated as a part of the statistical processing of the "flat" region. Additionally, the integral for plateau and the integral for the whole profile were calculated. On their base, the plateau/multi ratio was determined, also for all cases.

Additionally, the fifth case, named "extended N^+" was introduced to the evaluation. In this case, the nitrogen implantation with the smallest ion energy value for N_2^+, i.e. 5 keV, was added to the set of all data for N^+.

RESULTS AND DISCUSSION

Fig. 1 presents the modelled values of the peak volume dopant concentrations, projected range, range straggling, kurtosis and skewness as functions of the acceleration voltage. All data are marked with appropriate symbols. The symbols for the ion energy of 5 keV in the extended N^+ case are marked with a dotted contour. The trend lines calculated by the spreadsheet are marked by solid lines for N^++N_2^+, ACS, N^+ and N_2^+ and by a dotted line - for the extended N^+.

It is seen that the acceleration voltage dependence of the peak volume dopant concentrations is close to logarithmic, while the same relations for the others - are close to a linear. The equations for all dependencies are shown in Table 2. Additionally, the values of the coefficient of determination R^2 are presented. Its value close to 1 indicates high compliance of the modelled results with the adopted trend.

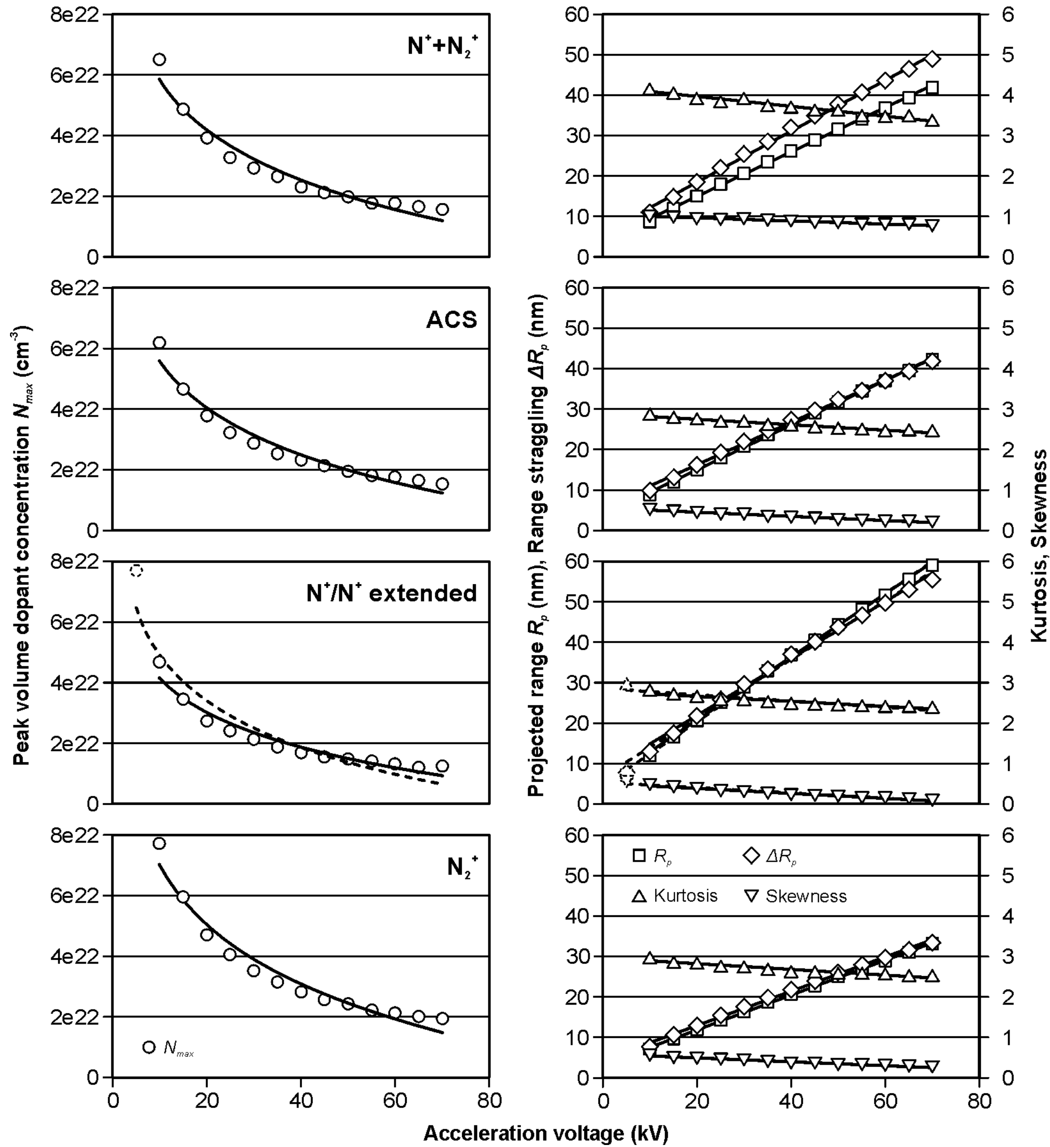

Figure 1. The graphical presentation of the modelled results with the calculated trend lines

The greatest values of the peak volume dopant concentrations appear for N_2^+ ions, because the energy of the implanted ions is the smallest in this case (the depth profiles are higher and narrower for lower energies) and the smallest - for N^+. The smallest values of the projected range and the range straggling are also for N_2^+ case, for the same reason. The kurtosis and the skewness are the largest for the direct beam, consisting of N^+ and N_2^+ ions. For all other cases, these parameters are smaller and similar to one another.

Fig. 2 shows the form of the multi-profiles for all considered cases with the implanted fluence of 1e17 cm^{-2}. Additionally, all component profiles and the appropriate implanted fluences are shown. The determined "flat" region is marked in gray. The longer platea as well as smaller concentrations are visible for N^+ and N^+ extended cases. The shortest plateau is observed for N^++N_2^+ beam. ACS profile is not a good direct beam equivalent.

Table 2. The trend line equations and the coefficient of determination values for all considered cases

Parameter	Trend line equation	Coefficient of determination
	N^++N_2^+	
N_{max}	$y=-2e22\ln(x)+1e23$	$R^2=0.9575$
R_p	$y=0.5498x+3.9088$	$R^2=0.999$
ΔR_p	$y=0.6303x+5.9407$	$R^2=0.997$
Kurtosis	$y=-0.0179x+4.2053$	$R^2=0.9547$
Skewness	$y=-0.0054x+1.0315$	$R^2=0.9723$
	ACS	
N_{max}	$y=-2e22\ln(x)+1e23$	$R^2=0.9606$
R_p	$y=0.5537x+3.9429$	$R^2=0.9991$
ΔR_p	$y=0.5257x+5.6945$	$R^2=0.997$
Kurtosis	$y=-0.0101x+2.8887$	$R^2=0.9454$
Skewness	$y=-0.0078x+0.5516$	$R^2=0.9818$
	N^+	
N_{max}	$y=-2e22\ln(x)+8e22$	$R^2=0.9477$
R_p	$y=0.7799x+5.1659$	$R^2=0.9989$
ΔR_p	$y=0.7053x+7.7429$	$R^2=0.9953$
Kurtosis	$y=-0.0063x+2.7864$	$R^2=0.901$
Skewness	$y=-0.006x+0.5016$	$R^2=0.9751$
	N^+ extended	
N_{max}	$y=-2e22\ln(x)+1e23$	$R^2=0.914$
R_p	$y=0.7911x+4.6044$	$R^2=0.9984$
ΔR_p	$y=0.7251x+6.7516$	$R^2=0.9935$
Kurtosis	$y=-0.0076x+2.8497$	$R^2=0.853$
Skewness	$y=-0.0065x+0.5263$	$R^2=0.961$
	N_2^+	
N_{max}	$y=-3e22\ln(x)+1e23$	$R^2=0.9608$
R_p	$y=0.4303x+3.2945$	$R^2=0.9992$
ΔR_p	$y=0.4226x+4.5407$	$R^2=0.9968$
Kurtosis	$y=-0.0139x+2.9603$	$R^2=0.9289$
Skewness	$y=-0.0093x+0.5776$	$R^2=0.9817$

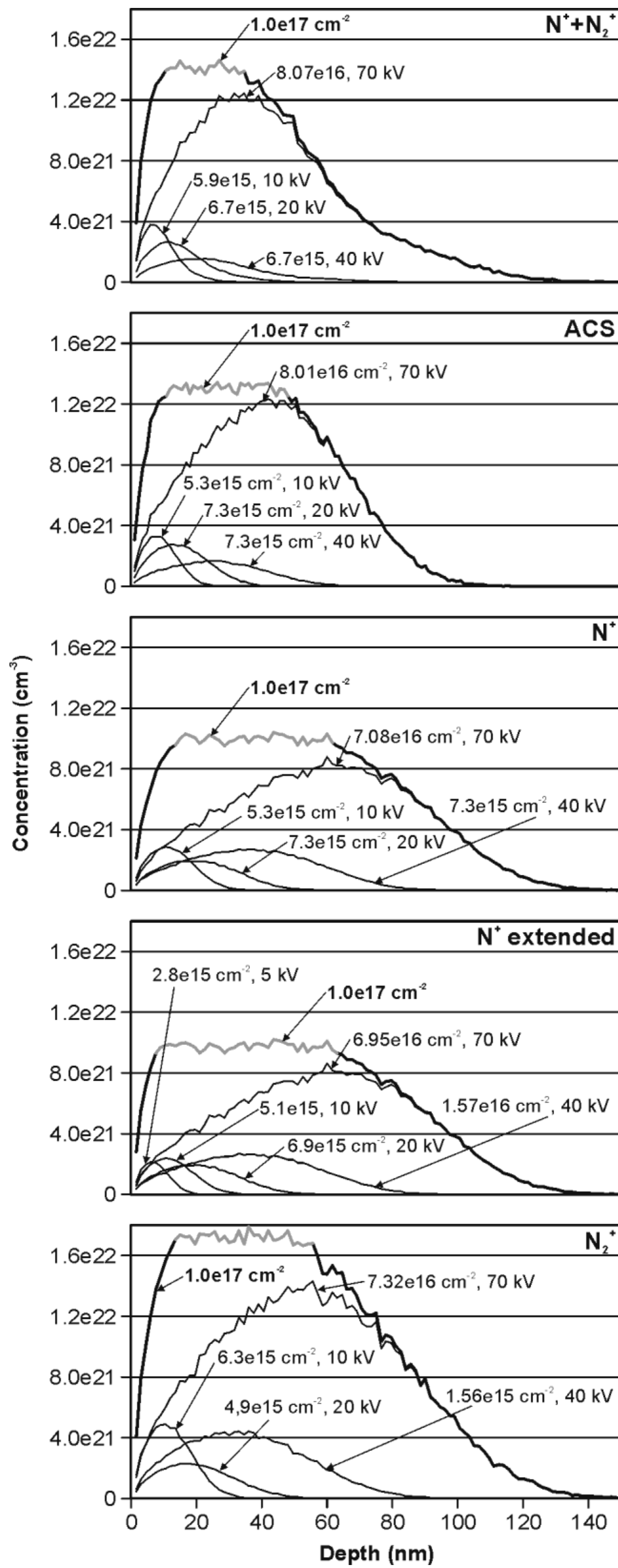

Figure 2. The multi-profiles and the component profiles with the implanted fluences

The bar charts, shoving the values and trends for the thickness of plateau, the average value of this thickness (average concentration for flat region), the standard deviation and the standard error of the concentration are presented in Fig. 3.

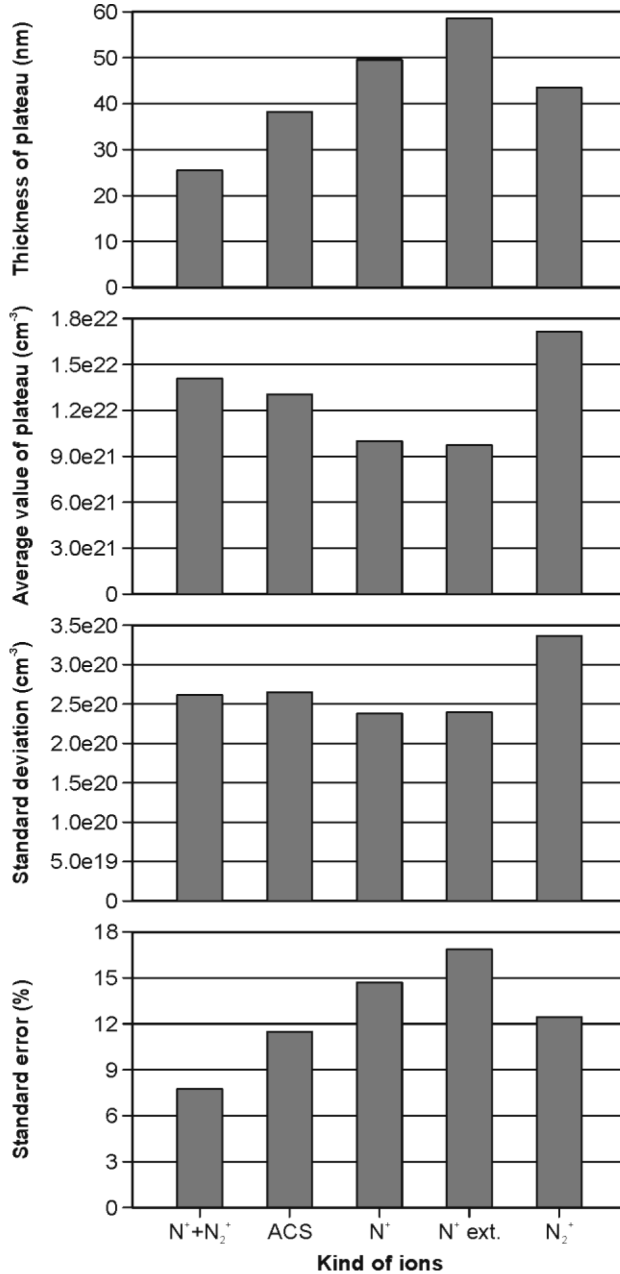

Figure. 3. The thickness of plateau, the average value of the plateau, the standard deviation and standard error values and the trends for all considered cases

It is seen that the plateau thickness is the greatest for extended N^+ case. This value is more than twice as large as the plateau thickness for N^++N_2^+ beam. The average value of the plateau is the smallest for extended N^+ case and the greatest - for N_2^+ ions. The similar trends are for the

standard deviation, however in this case, the deviation between different results is much smaller. The standard error is the smallest for nitrogen direct beam and the greatest - for N^+ extended case. The difference is more than two fold. All values for ACS are different in comparison to the values determined for N^++N_2^+ beam, especially for the thickness of the plateau and the standard error.

Fig. 4 shows the values and the trend of the integral for the plateau, the integral for the multi and the plateau/multi ratio. The greatest plateau share in multi-profile is for N^+ extended case and it is about 35% and the smallest - for N^++N_2^+ beam (about 17%). Also ACS values are different in comparison to N^++N_2^+ case. The difference is the greatest for the plateau/multi ratio.

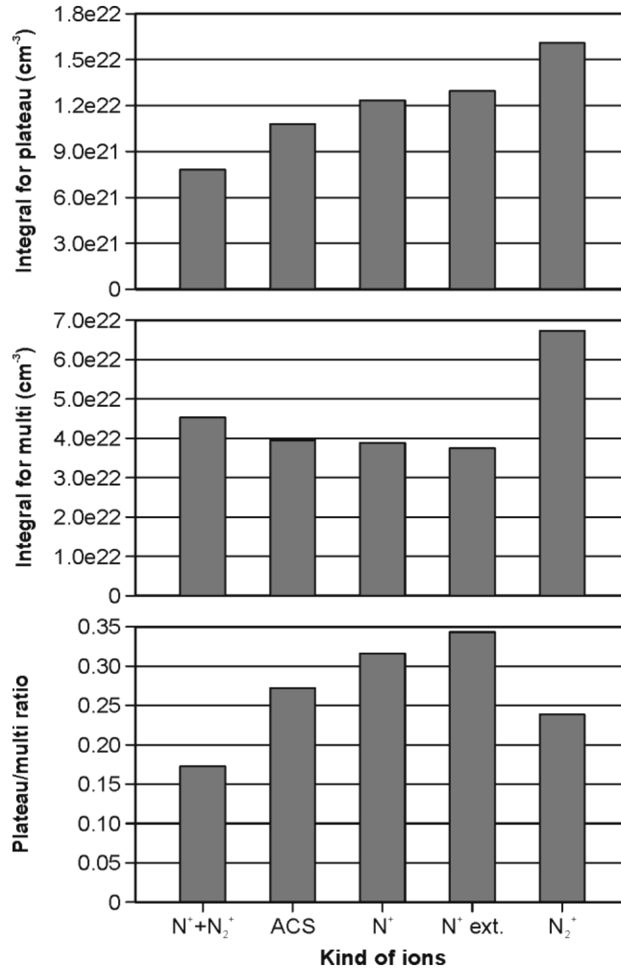

Figure 4. The integral for the plateau, the integral for the multi and the plateau/multi ratio values and the trends for all considered cases

CONCLUSION

On the basis of the results on the modelling/determining of the multi-energy ion implantation we can conclude as follows:

1. The ion beam without mass separation is less effective in comparison to the beams with mass separation. The plateau thickness for N^++N_2^+ ions was about two times smaller than for N^+.

2. The effectiveness of the mass separated beams depends on the type of the used ions. For example, the plateau thickness for N^+ ions was about 14% thicker than for N_2^+ ions.
3. The effectiveness can be increased by applying the extended process. For example, one additional process, extended multi-implantation of N^+ can increase the plateau thickness by approximately 20%.
4. ACS profiles deviate from reality and are not a good equivalent for multi-implantation using the ion beams without mass separation.
5. The average value of the plateau, i.e. average concentration of the flat region depends on the type of used ions. This relationship should be taken into account when designing the concentration level of the implanted element.
6. The best results are obtained for extended N^+ multi-implantation case. The thickness of the plateau is the largest and the plateau/multi ratio is the most favourable. Unfortunately, the standard error value is also the largest.

REFERENCES

1. ARAI N., TSUJI H., NAKATSUKA H., KOJIMA K., ADACHI K., KOTAKI H., ISHIBASHI T., GOTOH Y., ISHIKAWA J., 2008: Germanium nanoparticles formation in silicon dioxide layer by multi-energy implantation of Ge negative ions and their photo-luminescence, Materials Science and Engineering B 147, 230–234.
2. BARLAK M., WILKOWSKI J., WERNER Z., 2016: Ion implantation changes of tribological and corrosion resistance properties of materials used in wood industry, Annals of Warsaw University of Life Science – SGGW, Forestry and Wood Technology 94, 19–27.
3. BARLAK M., WILKOWSKI J., BORUSZEWSKI P., WERNER Z., PAŁUBICKI B., 2017: Changes of functional properties of materials used in wood industry after ion implantation processes, Annals of Warsaw University of Life Science – SGGW, Forestry and Wood Technology 97, 133–139.
4. BARLAK M., WILKOWSKI J., WERNER Z., 2019a: Modelling of the ion implantation modification of WC-Co indexable knives for wood machining, Annals of Warsaw University of Life Science – SGGW, Forestry and Wood Technology 106, 57–61.
5. BARLAK M., WILKOWSKI J., SZYMANOWSKI K., CZARNIAK P., PODZIEWSKI P., WERNER Z., ZAGÓRSKI J., STASZKIEWICZ B., 2019b: Influence of the ion implantation of nitrogen and selected metals on the lifetime of WC-Co indexable knives during MDF machining, Annals of Warsaw University of Life Science – SGGW, Forestry and Wood Technology 108, 45–52.
6. BARLAK M., WILKOWSKI J., WERNER Z., 2019c: Modelling of nitrogen implantation processes into WC-Co indexable knives for wood-based material machining using ion implanters with or without direct ion beam, Annals of Warsaw University of Life Science – SGGW, Forestry and Wood Technology 108, 68–78.
7. BARLAK M., WILKOWSKI J., WERNER Z., 2019d: The selected problems of the modelling of the depth profiles of the elements implanted to the tools used in wood material machining, Biuletyn Informacyjny OB-RPPD 3-4, 118–134, in Polish.
8. BECERRA H.M., Gloria V.V., LIZÁRRAGA-MEDINA E.G., RANGEL-ROJO R., SALAZAR D., OLIVER A., 2017: Development of optical waveguides through multiple-energy ion implantations, Ion Implantation - Research and Application 101–123.

9. BONNY K., DE BAETS P., PEREZ Y., VLEUGELS J., LAUWERS B., 2010: Friction and wear characteristics of WC-Co cemented carbides in dry reciprocating sliding contact, Wear 268, 1504–1517.
10. CHEN H.-Y., LIN Y.-S., 2019: Enhancement of second-harmonic generation in thermally poled fused silica by multi-energy argon ion implantation, Optical Materials 95, 109217.
11. CHOI S.-H., KANG S.-D., KWON Y.S., LIM S.G., CHO K.K., AHN I.-S., 2010: The effect of sintering conditions on the properties of WC-10wt%Co PIM compacts, Research on Chemical Intermediates 36, 743–748.
12. DAVID M.L., RATCHENKOVA A., OLIVIERO E., DENANOT M.F., BEAUFORT M.F., DECLÉMY A., BLANCHARD C., GERASIMENKO N.N., BARBOT J.F., Radiation damage in He implanted silicon at high temperature using multi-energies, Nuclear Instruments and Methods in Physics Research B 198, 83–89.
13. DENING W., WEIYUAN W., 1987: A study of multi-energy ion implantation, Journal of Electronics 4, 39-45.
14. FAYEULLE S., TREHEUX D., GUIRALDENQ P., 1986: Nitrogen implantation in tungsten carbides, Journal of Materials Science 21, 1814–1818.
15. FU G., WANG K.-M., WANG X.-L., LU F., LU Q.-M., SHEN D.-Y., MA H.-J., NIE R., 2007: Formation of planar optical waveguide by multi energy Si ion implantation into Nd:YVO_4 crystal, Surface and Coatings Technology 201, 5427–5430.
16. LAZAR M., LAARIEDH F., CREMILLIEU P., PLANSON D., LECLERCQ J.-L., 2015: The channelling effect of Al and N ion implantation in 4H–SiC during JFET integrated device processing, Nuclear Instruments and Methods in Physics Research B 365, 256–259.
17. LIU X.-H., ZHAO J.-H., ZHANG S.-M., PENG B.-G., CHEN M., MING X.-B., MAC Y.-J., QIN X.-F., 2012: Damage behaviours in Nd:YVO_4 by multi-energy proton implantation, Nuclear Instruments and Methods in Physics Research B 286, 213–217.
18. LIU T., KONG W.-J., QIAO M., CHENG Y., 2018: Maintain Raman property in ZnS single crystal waveguide formed by multienergy He ion implantation at 633 nm, Results in Physics 11, 822-825.
19. MAGRUDER III R.H., WELLER R.A., WEEKS R.A., WEHRMEYER J., ZUHR R.A., HENSLEY D.K., 2001: Effects of ArF excimer irradiation on single energy and multi energy Ge ion implanted silica, Journal of Non-Crystalline Solids 280, 169–176.
20. MAGRUDER III R.H., WEEKS R.A., WELLER R.A., ZUHR R.A., 2002: Effects of multi-energy Si and O ion implantation on the optical properties of silica, Journal of Non-Crystalline Solids 304 224–232.
21. MAGRUDER III R.H., WEEKS R.A., WELLER R.A., 2003: Luminescence and absorption in type III silica implanted with multi-energy Si, O and Ar ions, Journal of Non-Crystalline Solids 322, 58–67.
22. MAGRUDER R.H., WEEKS R.A., WELLER R.A., GALYON R., 2004: Photoluminescence and absorption in multi-energy Ge implanted type III silica, Journal of Non-Crystalline Solids 345-346, 284–292.
23. MAGRUDER III R.H., WEEKS R.A., MORIMOTO Y., 2011: Si related defects in the VUV in silicon multi-energy implanted type III silica, Nuclear Instruments and Methods in Physics Research B 269 2532–2538.

24. MIKKELSEN N.J., PEDERSEN J., STRAEDE C.A., 2002: Ion implantation - the job coater's supplement to coating techniques, Surface and Coatings Technology 158–159, 42–47.
25. MILMAN. YU.V., CHUGUNOVA S., GONCHARUCK V., LUYCKX S., NORTHROP I.T., 1997: Low and high temperature hardness of WC-6 wt%Co alloys, International Journal of Refractory Metals and Hard Materials 15, 97–101.
26. NAUMOVA O.V., ANTONOVA I.V., POPOV V.P., STAS V.F., 2003: Heterostructures formed on silicon by high-dose multi-energy hydrogen implantation, Microelectronic Engineering 66, 422–426.
27. OLOVSJÖ S., JOHANSON R., FALSAFI F., BEXELL U., OLSSON M., 2013: Surface failure and wear of cemented carbide rock drill buttons - The importance of sample preparation and optimized microscopy settings, Wear 302, 1546–1554.
28. PHELPS G.J., 2004: Dopant ion implantation simulations in 4H-silicon carbide, Modelling and Simulation in Materials Science and Engineering 12, 1139–1146.
29. PIEKOSZEWSKI J., KEMPIŃSKI W., BARLAK M., WERNER Z., ŁOŚ S., ANDRZEJEWSKI B., STANKOWSKI J., PIEKARA-SADY L., SKŁADNIK-SADOWSKA E., SZYMCZYK W., KOLITSCH A., GRÖTZSCHEL R., STAROSTA W., SARTOWSKA B., 2009: Superconductivity of Mg–B layers prepared by a multi-energy implantation of boron into magnesium and magnesium into boron bulk substrates followed by the furnace and pulsed plasma annealing, Surface and Coatings Technology 203, 2694–2699.
30. PIRSO J., LETUNOVITŠ S., VILJUS M., 2004: Friction and wear behaviour of cemented carbides, Wear 257, 257–265.
31. POSSELT M., MÄDER M., LEBEDEV A., GRÖTZSCHEL R., 2005: Multiple implantations into Si: Influence of the implantation sequence on ion range profiles, Applied Physics Letters 87, 043109.
32. RODRIGUEZ R.J., GARCIA J.A., SANCHEZ R., PEREZ A., GARRIDO B., MORANTE J., 2002: Modification of surface mechanical properties of polycarbonate by ion implantation, Surface and Coatings Technology 158–159, 636–642.
33. SHEIKH-AHMAD J.Y., BAILEY J.A., 1999: High-temperature wear of cemented tungsten carbide tools while machining particleboard and fibreboard, Journal of Wood Science 45, 445-455.
34. STRAEDE C.A., 1996: Application of ion implantation in tooling industry, Nuclear Instruments and Methods in Physics Research B 113, 161–166.
35. TERANISHI N., FUSE G., SUGITANI M., 2018: A review of ion implantation technology for image sensors, Sensors 18, 2358.
36. TSUJI H., ARAI N., GOTOH N., MINOTANI T., KOJIMA K., ADACHI K., KOTAKI H., ISHIBASHI T., GOTOH Y., ISHIKAWA J., 2007: Germanium nanoparticles formed in silicon dioxide layer by multi-energy implantation and oxidation state of Ge atoms, Journal of Physics: Conference Series 61 1196–1201.
37. WANG D., CHEN Z.Q., ZHOU F., LU W., MAEKAWA M., KAWASUSO A., 2009: Ferromagnetism and microstructure in Fe^+-implanted ZnO, Applied Surface Science 255 9371–9375.

38. WANG J., ZHANG X., FANG F., CHEN R., 2019: Diamond cutting of micro-structure array on brittle material assisted by multi-ion implantation, International Journal of Machine Tools and Manufacture 137, 58–66.
39. WERNER Z., SZYMCZYK W., PIEKOSZEWSKI J., SEAH M.P., RATAJCZAK R., NOWICKI L., BARLAK M., RICHTER E., 2009: Stoichiometric MgB_2 layers produced by multi-energy implantation of boron into magnesium, Surface and Coatings Technology 203, 2712–2716.
40. ZHANG S.-M., CAI L.-T., LIU Q.-X., LIU X.-H., MING X.-B., 2013: Optical waveguide in stoichiometric lithium niobate by multi-low-energy helium ion implantation, Nuclear Instruments and Methods in Physics Research B 307, 438–441.
41. ZHANG Z.J., NARAMOTO H., MIYASHITA A., STRITZKER B., LINDNER J.K.N., 1998: Low-temperature epitaxial growth of β-SiC by multiple-energy ion implantation, Physical Review B 58, 12652–12654.
42. ZHAO J.-H., WANG X.-L., CHEN F., 2010: 1×4-Branch waveguide power splitters in lithium niobate by means of multi-energy O ion implantation, Optical Materials 32, 1441–1445.
43. ZHAO J., YE L., LIU Y., LI S., FU G., YUE Q., 2019: Optical properties and surface blistering visualization on multiple-energy He-implanted Yb:YGG crystal by annealing treatment, Results in Physics 15, 102621.

Streszczenie: *Modelowanie multiimplantacji jonów azotu do wymiennych noży WC-Co, stosowanych w obróbce materiałów drzewnych.* W artykule przedstawiono wyniki modelowania procesów multiimplantacji jonów azotu do wymiennych noży WC-Co, stosowanych w obróbce materiałów drzewnych. Modelowanie przeprowadzono dla implantacji jonów N^{+}+N_2^{+} (dla implantatorów z separacją masową) oraz N^{+} i N_2^{+} (dla implantatorów bez separacji masowej). Dodatkowo, zostały przedstawione wyniki modelowania dla średniej krotności jonizacji oraz dla przypadku rozszerzonej implantacji. Najlepsze wyniki, tj. najdłuższy obszar plateau oraz najkorzystniejszy stosunek plateau do całości głębokościowego profilu uzyskano dla jonów N^{+}.

Corresponding author:

Marek Barlak
e-mail: marek.barlak@ncbj.gov.pl
National Centre for Nuclear Research Świerk - NCBJ
Plasma/Ion Beam Technology Division (FM2)
7 Andrzeja Sołtana St.
05-400 Otwock, Poland